frontiers | Frontiers in Materials

TYPE Original Research
PUBLISHED 14 February 2024
DOI 10.3389/fmats.2024.1363474

OPEN ACCESS

EDITED BY
Leilei Chen,
Southeast University, China

REVIEWED BY
Fen Ye,
Tongji University, China
Chuanqi Yan,
Southwest Jiaotong University, China

*CORRESPONDENCE
Bangyan Hu,
hubangyan@xju.edu.cn

RECEIVED 30 December 2023
ACCEPTED 25 January 2024
PUBLISHED 14 February 2024

CITATION
Hu B, Ai X and Feng J (2024), Comparative study of typical asphalt binders in Xinjiang region modified with warm mix additives. *Front. Mater.* 11:1363474. doi: 10.3389/fmats.2024.1363474

Comparative study of typical asphalt binders in Xinjiang region modified with warm mix additives

Bangyan Hu[1,2]*, Xianchen Ai[2,3] and Juan Feng[1]

[1]College of Civil Engineering and Architecture, Xinjiang University, Urumqi, China, [2]Xinjiang Key Laboratory of Green Construction and Smart Traffic Control of Transportation Infrastructure, Urumqi, China, [3]School of Traffic and Transportation Engineering, Xinjiang University, Urumqi, China

Xinjiang's representative asphalt binders, such as Karamay and Tahe asphalt, lack sufficient research on warm-mix additive modification effects. Given their unique microstructure and molecular composition differences, comprehensive investigations are essential for a nuanced understanding of these binders. This study added Sasobit and Evotherm warm mix additives to Karamay 90# asphalt and Tahe 90# asphalt, respectively. The evaluation of diverse warm mix additives' impact on diverse asphalt binders involved viscosity, softening point, penetration tests, Fourier transform infrared (FTIR) and analysis of saturate, aromatic, resin, and asphaltene (SARA) fractions. Additionally, molecular models of asphalt were constructed using Materials Studio software, based on the SARA test data. Molecular models of Sasobit and Evotherm were also developed, representing organic wax and a cationic quaternary ammonium surfactant, respectively. Conducting molecular dynamics simulations of warm mix additives and two asphalt molecules yielded valuable insights into solubility parameters and the radial distribution function (RDF). This approach enabled a thorough and comparative exploration of the modification mechanisms employed by various warm mix additives on different asphalt types at a molecular scale. The results indicate that, Evotherm excelled in enhancing high-temperature asphalt performance, while Sasobit surpassed it in low-temperature. The viscosity reduction by Sasobit proved more effective for K90, while for T90 asphalt, the trend was reversed with Evotherm exhibiting superior performance. The solubility parameter in MD simulations consistently correlates with asphalt viscosity results. Sasobit showed enhanced compatibility with K90 asphalt, while T90 asphalt demonstrated greater suitability for modification with Evotherm.

KEYWORDS

warm mix asphalt, Xinjiang asphalt binders, FTIR, SARA, Molecular dynamics simulation

1 Introduction

Positioned in China's northwest, Xinjiang plays a pivotal role in connecting China and Central Asia through the "Belt and Road" initiative (Transport, E. D. O. C. J. O. H. A., 2020). Its robust transportation sector amplifies infrastructure needs in the carbon-neutral era (Chen et al., 2023a; Cheng et al., 2023). Low-carbon technologies were actively pursued by industries for a green transformation, while strategies for low-carbon and decarbonization

TABLE 1 Technical indicators of the base asphalt binder.

Indicator	Unit	K90 Test data	T90 Test data	Technical requirements
Penetration (25°C,5°s,100 g)	0.1 mm	96.9	92.2	80–100
Penetration indexPI	—	−0.3692	0.5079	−1.5–1.0
Softening point (TR&B)	°C	53.6	67.5	≥45
Ductility (10°C)	cm	123.1	>150	≥20
Ductility (15°C)	cm	131.7	>150	≥100
Density	(g/cm^3)	0.981	1.024	Measurement records
After TFOT (5 h,163°C)				
Mass loss	%	−0.181	−0.359	±0.8
Residual penetration ratio	%	57.0	64.3	≥57
Residual Ductility (10°C)	cm	27.5	>150	≥8
Residual Ductility (15°C)	cm	65.9	>150	≥20

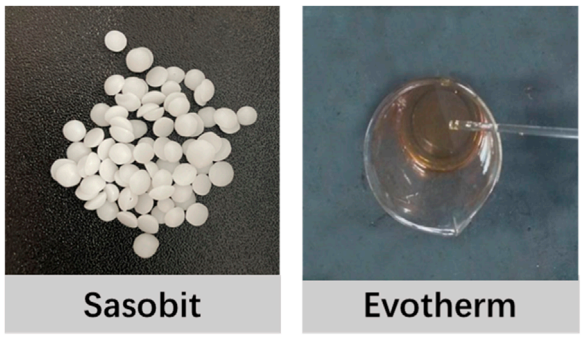

FIGURE 1
Asphalt warm mix additives.

are explored by the road building sector (Zhang L. et al., 2023; Chen et al., 2023b). Among these approaches, warm-mix asphalt (WMA) emerges as a potent method for reducing energy consumption (Rubio et al., 2012). In contrast to traditional hot-mix asphalt, WMA involved lower temperatures in mixing, paving, and compaction. This conserves fuel and reduces emissions of harmful gases and smoke (Kim et al., 2011). Furthermore, the occurrence of severe thermal aging in asphalt binders during the construction process was mitigated (Banerjee et al., 2012).

Xinjiang, endowed with abundant oil and gas resources, features Karamay asphalt (KLMY) and Tahe asphalt (TH) as its most representative petroleum products. KLMY known for its high production and convenient transportation, has been extensively utilized in road construction throughout Xinjiang (Wang et al., 2022). The chemical composition of KLMY notably differed from the commonly used road petroleum asphalt in China, exhibiting characteristics such as minimal wax content, elevated resins content, and extremely low asphaltene content (Gao et al., 2022). Consequently, exceptional performance was exhibited in low temperatures, resistance to aging, and fatigue. Nevertheless, KLMY's unique composition, notably its limited compatibility with commonly employed modifiers, especially high-molecular-weight polymer modifiers, presents challenges in preparing modified asphalt (Yu et al., 2018; Yu et al., 2019). In contrast, TH another petroleum asphalt variety produced in Xinjiang, diverged from KLMY. With a significantly higher asphaltene content than commonly used road petroleum asphalt, TH excels in high-temperature performance but exhibited poorer low-temperature ductility, coupled with a relatively lower price (Ning et al., 2015). In practical engineering in Xinjiang, there was widespread reliance on asphalt from other provinces or imports for modification, hindering cost control and large-scale application. Consequently, a focus has been placed by researchers on investigating the mechanistic aspects of modifying Xinjiang asphalt to develop WMA tailored to the region (Jiang et al., 2021).

To address the challenge of inadequate stability between WMA and asphalt binders, the focus has been primarily placed on the structural mechanisms of asphalt, modification processes, and comprehensive performance evaluation by researchers (Oyan, 2022). In this pursuit, three main groups are identified for categorizing WMA additives: organic additives, foaming processes and additives, and chemical additives. Another approach involves the combination of two or more of the aforementioned methods to reduce binder viscosity (Jiang et al., 2021). In a study conducted by Sengoz et al., the physical and rheological properties of asphalt were examined with the inclusion of natural or synthetic zeolites. The study revealed that the asphalt stiffness and temperature susceptibility demonstrated an increase after the introduction of zeolite. However, as a hydrophilic inorganic material, zeolite demonstrated poor compatibility with asphalt, resulting in its

TABLE 2 Basic information and preparation process of WMA.

WMA additive	Content (% by weight)	Preparation process	Karamay asphalt ID	Tahe asphalt ID
Sasobit	1%, 2%, 3%, 4%, and 5%	Sheared for 20 min (160°C, 3000 rpm)	KS1, KS2, KS3, KS4, KS5	TS1, TS2, TS3, TS4, TS5
Evotherm	0.2%,0.4%, 0.6%, 0.8%, and 1%	Sheared for 10 min (160°C, 600 rpm)	KE0.2, KE0.4, KE0.6,KE0.8,KE1	TE0.2, TE0.4, TE0.6, TE0.8, TE1

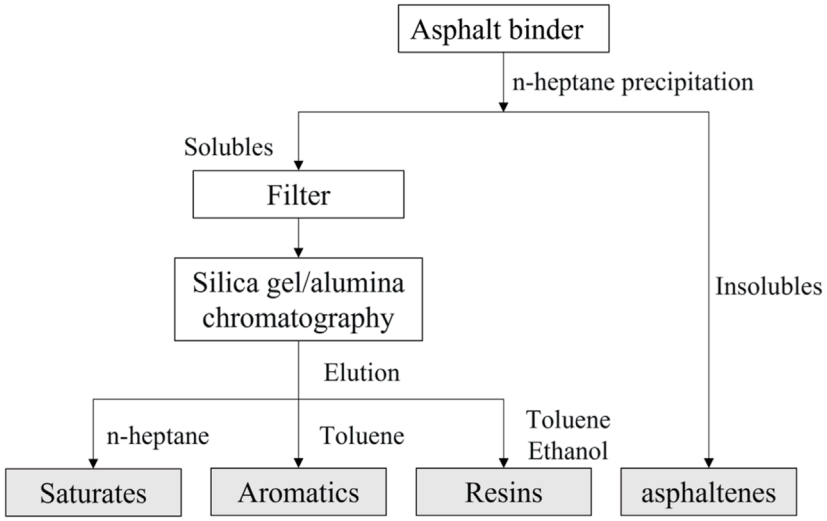

FIGURE 2
Corbett separation scheme.

poor dispersion in asphalt (Sengoz et al., 2013; Topal et al., 2014). Hossain et al. evaluated the effects of the addition of high quantities of paraffinic waxes to a base asphalt through rheological criteria. The shear viscosity and dynamic mechanical spectra indicate that wax perturbs the overall colloidal equilibrium of the base asphalt, thereby generating highly structured asphaltic materials (Hossain et al., 2013). Yu et al. modified crumb-rubber-modified asphalt with the addition of Sasobit and Evotherm, and the two products exhibited different responses in different content and situations. It was difficult to determine which product is better or what is the optimum content. Instead, the choice of the product and content highly depended on the environment, particularly the temperature, in which they were intended to be used (Yu et al., 2013).

Overall, the main reason for the poor stability in warm-mixed modified asphalt lay in the inadequate dispersion of the modifier in the asphalt and the unsuitability of the chosen modifier for the specific asphalt and engineering requirements. Despite scholars having extensively investigated the compatibility and stability of warm-mixed modified asphalt from process parameters to additives, research on the distinctive high-gel asphalt (Karamay asphalt) and high-asphaltene asphalt (Tahe asphalt) remained relatively limited.

Therefore, this study focused on two typical types of asphalt in Xinjiang, namely KLMY and TH. Two warm mix agents, Sasobit and Evotherm, were selected for investigation. The analysis involved examining the interactions between these agents and asphalt binders. The primary emphasis was on investigating the impact of varying application quantities on the fundamental properties of asphalt. Molecular dynamics (MD) simulation techniques were employed to analyze the viscosity reduction mechanisms of different warm mix agents in diverse asphalt compositions. This research aimed to offer crucial insights into the technology of WMA and base asphalt binder modification in Xinjiang.

TABLE 3 The wavenumber of each functional groups (Wen, 2010).

Functional group	Area of peak between (cm^{-1})
Asymmetrical stretching -CH_2-	2936–2916
Symmetrical stretching of -CH_2-	2863–2843
C=C stretch in aromatics	1642–1547
C-H asymmetric deform in CH_2 or CH_3	1490–1430
C-H symmetric deform in CH_3	1385–1365
= C-H bending vibration of benzene ring	900-800,830-800
C-H stretching in CH_2 or CH_3	764–650

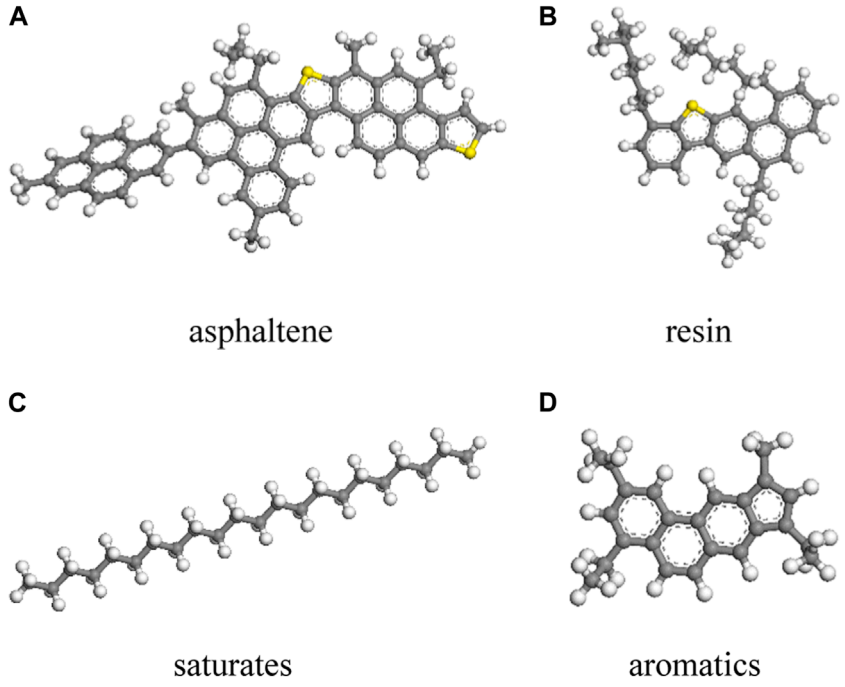

FIGURE 3
Asphalt molecules consist of these four components: **(A)** asphaltene, **(B)** resin, **(C)** saturates and **(D)** aromatics.

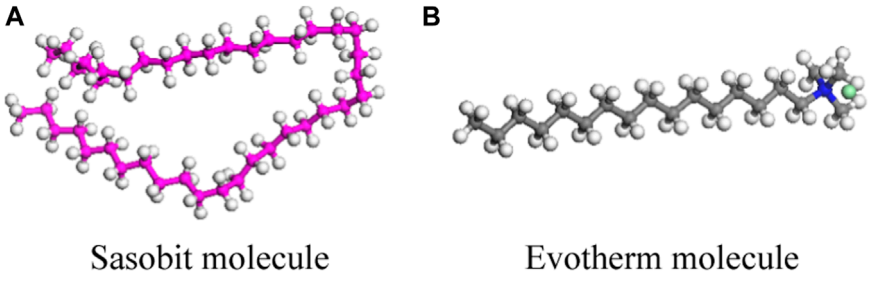

FIGURE 4
Molecular models of WMA additives: **(A)** Sasobit molecule and **(B)** Evotherm molecule.

2 Materials and methodology

2.1 Raw materials

2.1.1 Base asphalt

The base asphalt used in the research were KLMY90# asphalt (K90) and TH90# asphalt (T90), both produced by Sinopec Group. The basic properties of base asphalt were summarized in Table 1.

2.1.2 Warm-mix additives

In this study, two typical WMA additives, namely the wax-based WMA additive Sasobit and the surfactant WMA additive Evotherm, were employed. The visual representations of these additives can be observed in Figure 1. Sasobit, sourced from Sasol Chemicals in Nanjing, Jiangsu Province, China, exhibits a melting point of approximately 100°C and effectively liquefies in asphalt above this temperature. Evotherm, a patented product of MeadWestvaco in Shanghai, China, was employed in the form of Evotherm M1 in this study.

2.1.3 Warm mix asphalt binders

Considering the disparities in physical state (solid versus liquid) and mechanisms for viscosity reduction, Sasobit and Evotherm were incorporated into the asphalt using distinct mixing procedures. In the preparation of the WMA containing Sasobit, the base asphalt was heated to 160°C in an oil bath. Once the target temperature was reached, Sasobit pellets (1%, 2%, 3%, 4%, and 5% by mass of asphalt binder) were gradually added while the binder was stirred at a relatively low speed. Subsequently, stirring was continued for an additional 20 min at a speed of 3000 rpm to ensure the formation of a homogeneous binder.

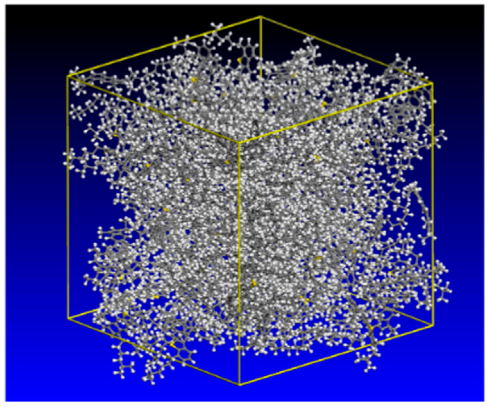

FIGURE 5
K90 asphalt molecular model.

In the formulation of the base asphalt containing Evotherm, the authors expressed concern that prolonged stirring (20 min) at 160°C could potentially compromise its functionality. Therefore, the blending time was restricted to 10 min. Table 2 outlines the key characteristics of the WMA additives and delineates the steps involved in preparing the WMA binders.

2.2 Test procedures

2.2.1 Physical indexes test

Asphalt property tests were performed on the asphalt samples, focusing primarily on penetration (at 15°C, 20°C, and 25°C), Brookfield rotational viscosity (at 90°C, 105°C, 120°C, 135°C, 150°C, and 165°C), ductility (at 10°C) and softening point assessments. The test procedures adhered to the guidelines outlined in the ASTM D5-06e1, ASTM D113-17, ASTM D4402-15, and ASTM D3461-18 standards, ensuring standardized and accurate measurements.

2.2.2 Corbett separation and colloidal index

The Corbett method has been widely employed in the fractionation of asphalt binder into saturates, aromatics, resin, and asphaltene (SARA) components (Xu et al., 2018b). This method utilizes solubility procedures and column chromatographic techniques to achieve the separation. A schematic representation of the Corbett separation process is illustrated in Figure 2.

The colloidal instability index (CII) serves as a metric to depict the intricate internal microstructure of binders (Masoumeh et al., 2016; Eltwati et al., 2022). According to the Gaestel theory, the presence of ample quantities of resins and aromatics can lead to the full peptization of asphaltenes, resulting in an effective mobility of micelles within asphalt (Siddiqui and Ali, 1999). CII is defined as the ratio of diffused components (aromatics and resins) to non-diffused compounds (saturates and asphaltenes). The following formula, Eq. 1, determines this parameter, proving to be highly useful for comparing different types of asphalt binders (Salehfard et al., 2021).

$$CII = \frac{(\text{Asphaltenes in wt\%}) + (\text{Saturates in wt\%})}{(\text{Resins in wt\%}) + (\text{Aromatics in wt\%})} \quad (1)$$

2.2.3 Fourier transform infrared (FTIR) test

The infrared spectrometer (IR), utilizing the selective absorption characteristics of the tested material for infrared radiation at different wavelengths, is an instrument employed for the analysis of molecular structures and chemical compositions. The FTIR has been recognized as a powerful tool for analyzing asphalt binders to determine functional groups, including carbonyl, hydroxyl, amine, amide, nitrile, ester, carboxylic, and aromatic groups (Brako and Wexler, 1963). The FTIR principle relies on the distinct vibration and rotation modes exhibited by various molecular bonds, which are identifiable through characteristic bands in the absorption spectrum of transmitted infrared radiation (Cheng et al., 2020). In this study, ATR-FTIR (Bruker VERTEX70) was utilized to identify the chemical functional groups of asphalt binders and their fractions. The scan ranged from 4,000 cm^{-1}–600 cm^{-1} with a 4 cm^{-1} resolution. To minimize experimental error, three replicates were tested for each specimen. Table 3 summarizes the typical peak positions of chemical functional groups.

2.3 Simulation models and methods

2.3.1 Construction of molecular model

(1) Asphalt Components

A molecular model of asphalt was constructed, providing input for Molecular Dynamic simulation. Two construction approaches were found in the literature: one involved an average model structure for the entire asphalt, and the other comprised a composition model consisting of several asphalt fractions (Chen et al., 2018). With advancements in experimental precision and an enhanced understanding of asphalt, researchers introduced asphalt models that exhibited higher levels of accuracy. In 2007, Zhang and Greenfield introduced a three-component model, utilizing two molecules to represent asphaltene, and one molecule each for resin and saturates (Zhang and Greenfield, 2007). Later, they put forth a four-component model (Zhang and Greenfield, 2008). In 2014, The 12 molecular models of SARA components proposed by Li and Greenfield, including SHRP AAA-1, AAK-1, and AAM-1, have been confirmed to be highly consistent with the real asphalt system (Li and Greenfield, 2014). In subsequent research, scholars in asphalt molecular modeling commonly adopted a twelve-molecule model (Li et al., 2022; Lu et al., 2022; Zhang J. et al., 2023). However, achieving consistency with experimental results became challenging when applying the 12 molecular models to allocate SARA, given the unique composition of Xinjiang asphalt. Hence, this paper adopted the four-molecule model proposed by Hansen in 2013 (Figures 3A–D) (Hansen et al., 2013). This relatively straightforward model has been demonstrated to predict the physical and rheological properties of asphalt binders in a general sense (Xu and Wang, 2016).

(2) Warm-Mix Additives

Sasobit® Sasol wax is a synthetic hydrocarbon hard wax obtained as by-product of the Fischer-Tropsch (FT) process, where hydrocarbons are synthesized from hydrogen and carbon monoxide. Sasobit has the molecular formula CnHn+2, and its long chain generally consists of 40–115 carbon atoms. Forty carbon atoms were selected to construct the Sasobit model (Figure 4A).

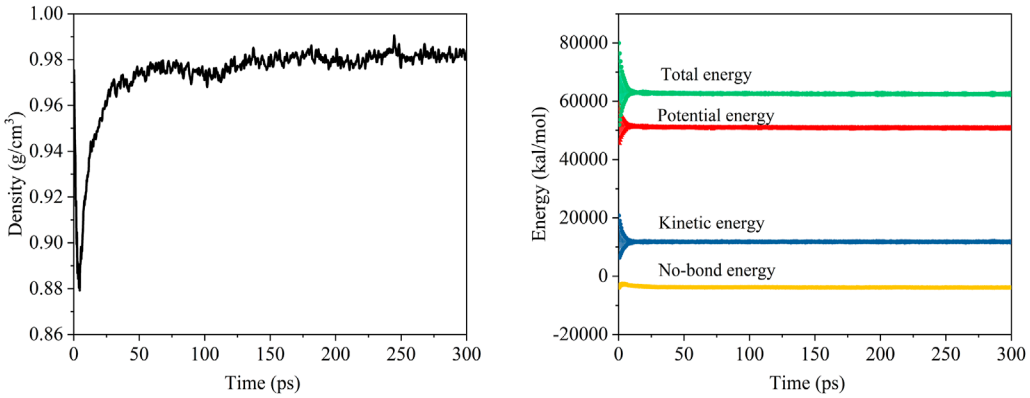

FIGURE 6
Density and energy curves of NPT equilibration process.

TABLE 4 Penetration correlation calculation table (Karamay asphalt).

ID	Penetration/0.1 mm			R^2	PI	T_{800}/°C	$T_{1.2}$/°C
	15°C	20°C	25°C				
K90	33.6	96.9	141.6	0.997	−0.369	47.32	−19.44
KS1	29.0	79.9	135.3	0.999	−0.699	47.38	−16.07
KS2	26.9	77.9	128.2	0.999	−0.811	47.49	−14.84
KK3	25.9	75.9	124.6	0.999	−0.867	47.53	−14.26
KS4	22.1	67.9	114.0	0.999	−1.137	47.61	−11.32
KS5	20.2	65.6	110.0	0.997	−0.345	49.27	−7.89
KE0.2	30.1	79.5	122.0	0.999	−0.131	49.81	−19.40
KE0.4	28.2	75.6	110.0	0.997	−0.016	51.13	−19.29
KE0.6	27.0	71.6	105.8	0.999	0.016	51.75	−19.02
KE0.8	26.1	69.5	101.0	0.998	0.050	52.24	−18.88
KE1	25.1	64.4	96.0	0.999	0.152	53.35	−18.87

Evotherm is a surfactant manufactured by MeadWestvaco (United States), and the surfactant is a patented product with an unknown molecular structure. However, Zhao pointed out that MeadWestvaco Company's third-generation product, Evotherm® M1, is a cationic quaternary ammonium surfactant (Zhao, 2012). Hence, in this paper, referencing literature (Wu et al., 2022), Cetyltrimethylammonium Chloride (CTAC), a cationic surfactant with the molecular formula $C_{19}H_{42}ClN$, was chosen to construct the Evotherm model, as shown in Figure 4B.

(3) Asphalt Molecular Model

The molecular model of the base asphalt was constructed according to the ratio the SARA fractions of asphalt using the Amorphous cell module in the Materials Studio; Taking the K90 as an example, as shown in the Figure 5.

2.3.2 Molecular dynamics simulation process

The Compass II force field in Materials Studio 2019 was employed in this paper. Prior to constructing the asphalt model, the component models and additive models were subjected to the Compass II force field and charges, and then underwent geometry optimization. The asphalt bulk model was created using the amorphous cell module, following 20,000 iterations of geometry optimization. A temperature range of 26.85°C–1526.85°C was established. Following geometry optimization and energy optimization, a subsequent annealing process was undertaken to refine the model, bringing it into closer approximation to the

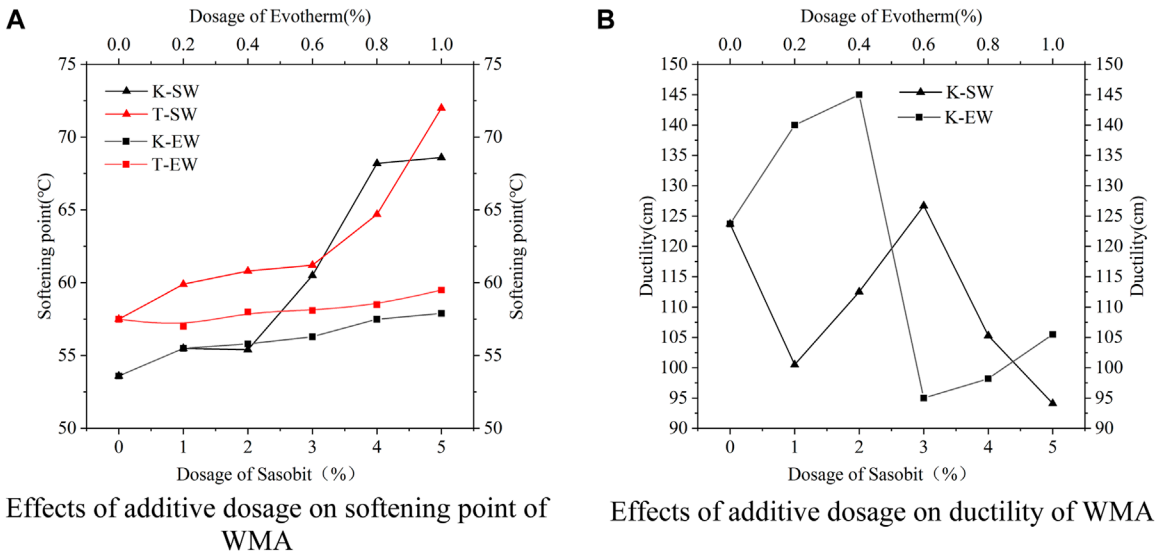

FIGURE 7
Softening point and ductility of WMA: **(A)** Softening point and **(B)** Ductility.

authentic molecular state (Yusuff et al., 2021). A 500ps dynamic equilibration simulation was conducted with the NVT ensemble (N = constant number of atoms, V = constant volume, and T = constant temperature) to transition the asphalt model from its initial state to an equilibrium state at normal temperature. Subsequently, a 500ps dynamic equilibration simulation was performed with the NPT ensemble (N = constant number of atoms, P = constant pressure, and T = constant temperature) at 1 atm to ensure that the system density matched real asphalt at 25°C. A final 500ps dynamic data collection simulation was executed to gather the required data. A Nose thermostat was employed during the dynamic equilibration process, and an Andersen thermostat was utilized in the dynamic data collection process. After the dynamic equilibration process and dynamic data collection process, all the models exhibited equilibrium density and equilibrium energy (Figure 6). To avoid data duplication, only the equilibrium curves after the NPT equilibration process of the K90 model was shown.

2.3.3 Quantitative analysis indicators

(1) Solubility Parameter

According to the derivation of Hildebrand et al.(Hildebrand and Scott, 1951), the solubility parameter enthalpy of mixing (ΔH_m) measures the compatibility of the materials and was calculated as Eqs 2–5.

$$\Delta H_m = \left[\frac{N_j V_j \cdot N_k V_k}{N_j V_j + N_k V_k}\right]\left[\delta_j - \delta_k\right] \tag{2}$$

$$\delta_j = \sqrt{\frac{\Delta E_j}{V_j}} \tag{3}$$

$$\delta_k = \sqrt{\frac{\Delta E_k}{V_k}} \tag{4}$$

$$\Delta\delta = \left|\delta_j - \delta_k\right| \tag{5}$$

The polymers j and k have relative molecular masses of N_j, N_k, their molar volumes are V_j and V_k, and their cohesive energy densities (CED) are $\frac{\Delta E_j}{V_{kj}}$ and $\frac{\Delta E_k}{V_k}$,respectively. The solubility parameters of the polymers are δ_j and δ_k, and the absolute values of the differences in solubility parameters is $\Delta\delta$.

Upon completing the processing of the Cohesive Energy Density task, the solubility parameters were obtained. A reduced difference between the solubility parameters for each molecular model indicate a higher compatibility between the two polymers.

(2) Radial distribution function

Radial distribution function (RDF) was used to quantify the cohesion between asphalt molecules in the MD. The molecular effects of warm-mix additives on cohesion can be further investigated using RDF.

The functional connection between the density and the distance from a reference point is described by the RDF, a statistical mechanics technique. The parameter g(r) Eq. 6 represents the probability of selected molecules in an asphalt molecule being at a distance from selected reference molecules and was used to define the aggregation behavior of asphalt molecules. The center of mass of the asphaltene was used as the reference point in this investigation.

$$g(r) = \frac{1}{4\rho\pi r^2 \xi r}\frac{\sum_{t=1}^{T}\sum_{j=1}^{N}\Delta N(r \to r + \xi r)}{N \times T} \tag{6}$$

where N = total number of molecules; T = total time of calculation (ps); r = distance from given reference point; ΔN = number of molecules within system interval; and ρ = system density.

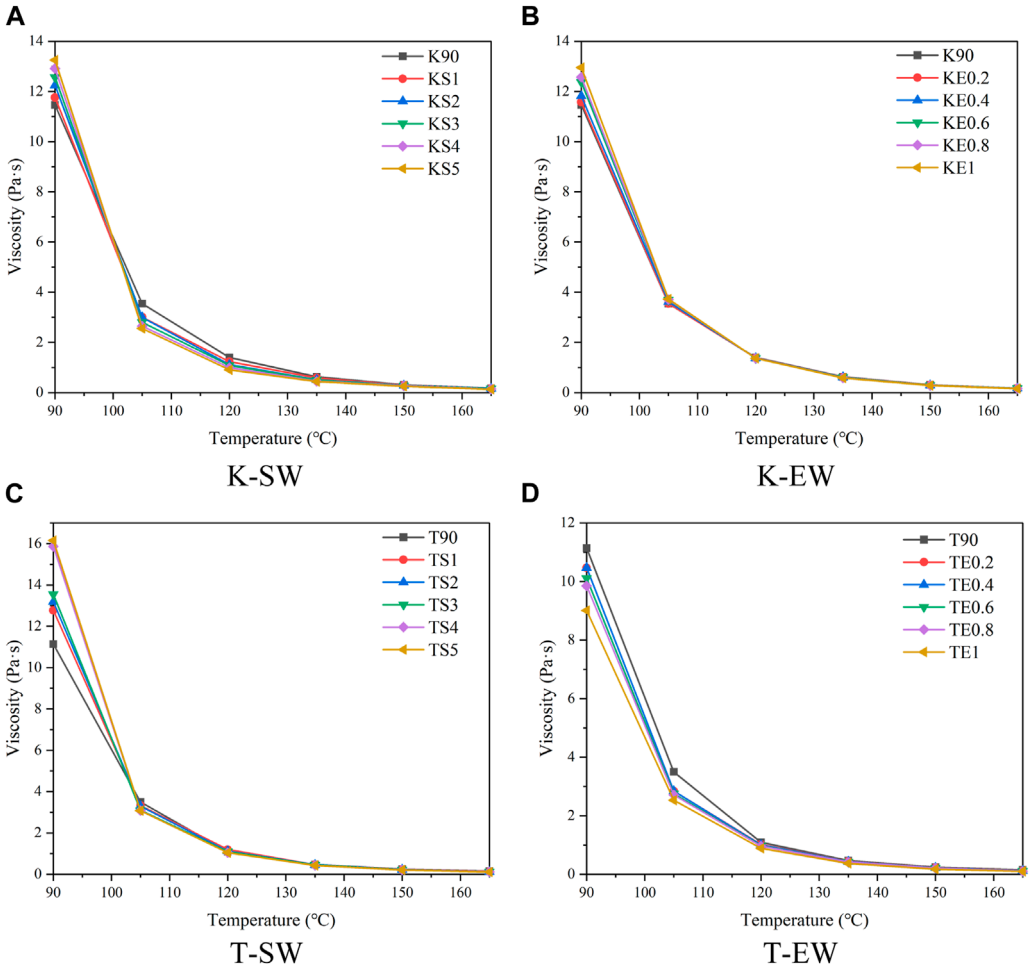

FIGURE 8
Variation curve of viscosity of base asphalt and WMA: **(A)** K-SW, **(B)** K-EW, **(C)** T-SW and **(D)** T-EW.

3 Results and discussion

3.1 Physical indexes analysis

3.1.1 Penetration analysis

According to the specifications outlined in JTG E20-2011(T0604-2011), logarithmic regression of penetration depth with temperature should be conducted as per Eq. 7. Subsequently, the penetration index (PI) was calculated using Eq. 8, the equivalent softening point (T_{800}) was determined via Eq. 9, the equivalent brittle point ($T_{1.2}$) was computed using Eq. 10, and the plastic temperature range (△T) was evaluated following Eq. 11. Detailed results were presented in Table 4 and Table 5.

$$\lg P = K + A_{\lg Pen} \times T \tag{7}$$

$$PI = \frac{20 - 500A_{\lg Pen}}{1 + 50A_{\lg Pen}} \tag{8}$$

$$T_{800} = \frac{\lg 800 - K}{A_{\lg Pen}} = \frac{2.9031 - K}{A_{\lg Pen}} \tag{9}$$

$$T_{1.2} = \frac{\lg 1.2 - K}{A_{\lg Pen}} = \frac{0.0792 - K}{A_{\lg Pen}} \tag{10}$$

$$\Delta T = T_{800} - T_{1.2} = \frac{2.8239}{A_{\lg Pen}} \tag{11}$$

Note: T is the test temperature of needle penetration, °C; P is the penetration value measured at each test temperature; A_{lgPen} is the coefficient of the regression equation. K is a constant term.

The thermal responsiveness of asphalt was illustrated by the PI, where an elevated value indicated reduced susceptibility to temperature fluctuations, while a diminished value signified heightened sensitivity. The T_{800} index reflected the asphalt's performance under high temperatures; a superior value conveyed excellent high-temperature attributes, while a lower value implied subpar performance in elevated conditions. The $T_{1.2}$ parameter was employed to evaluate the asphalt's resistance to low-temperature cracking. Additionally, the plastic temperature range ΔT was defined as the difference between T_{800} and $T_{1.2}$. This range was intricately linked to the temperature-sensitive characteristics of asphalt, serving as a direct manifestation of the material's applicable temperature spectrum.

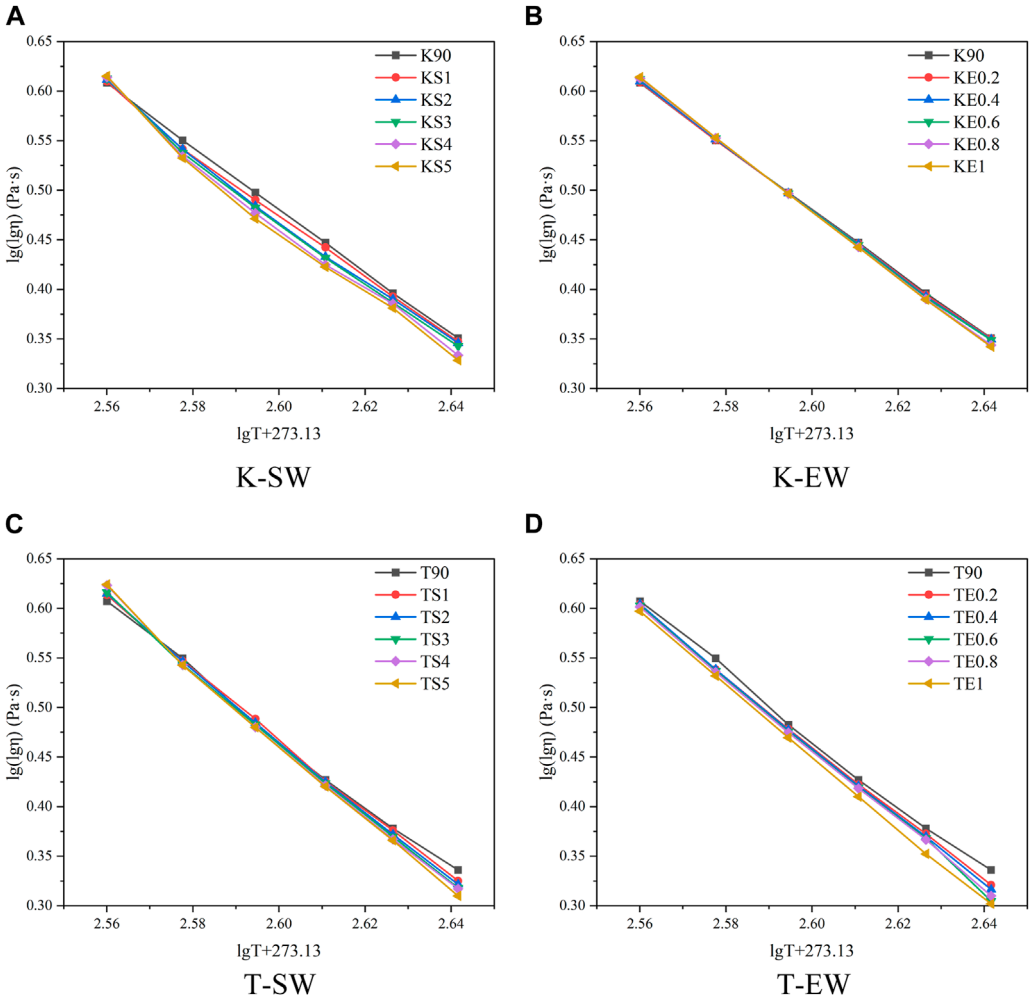

FIGURE 9
Viscosity temperature index relationship between base asphalt and WMA: **(A)** K-SW, **(B)** K-EW, **(C)** T-SW and **(D)** T-EW.

For Sasobit warm-mix modified Karamay asphalt (K-SW) and Tahe asphalt (T-SW), as well as Evotherm warm-mix modified Karamay asphalt (K-EW) and Tahe asphalt (T-EW), at temperatures of 15°C, 25°C, and 30°C, their penetration values were consistently lower than those of the base asphalt. With an increase in the dosage of warm-mix additives, the penetration values of the WMA gradually decreased. This indicated that the additives rendered the asphalt harder or increase its viscosity, thereby enhancing its resistance to deformation.

The PI values for K-SW and K-EW ranged from −1.5 to 0.5, while those for T-SW and T-EW fall within the ranged of −0.5 to 1.5. This suggests a certain relationship between the extent of temperature sensitivity improvement in WMA and the performance of the base asphalt. In the case of the two types of Xinjiang asphalt, the addition of Sasobit increased the asphalt's sensitivity to temperature, whereas Evotherm reduced its sensitivity to temperature. Additionally, an increase in the dosage of both warm-mix additives contributes to enhancing the temperature-sensitive performance of WMA.

With an increase in the dosage of both warm-mix additives, the T_{800} of WMA showed an upward trend, indicating that the warm-mix additives enhance the high-temperature performance of the two base asphalts. Specifically, KS5 exhibited a growth rate of 4.0%, KE1 showed a growth rate of 12.7%, TS5 experienced a growth rate of 3.3%, and TE1 demonstrated a growth rate of 4.7%. It was noteworthy that the improvement in high-temperature performance by Evotherm warm-mix additive was greater than that by Sasobit, and Karamay asphalt was more sensitive to changes in the type of warm-mix additive.

As the dosage of warm-mix additives increases, the $T_{1.2}$ of WMA gradually increases. The additives enhance the low-temperature performance of asphalt, with Sasobit showing a greater improvement in Karamay asphalt compared to Evotherm, while the trend was reversed for Tahe asphalt. It can be observed that the type of asphalt influences the choice of warm-mix additive.

3.1.2 Softening point analysis

The experimental results for the softening point of WMA were depicted in Figure 7A. The addition of WMA resulted in an increasing trend in the softening point of asphalt. With the increasing dosage of the additives, the softening point of K-SW

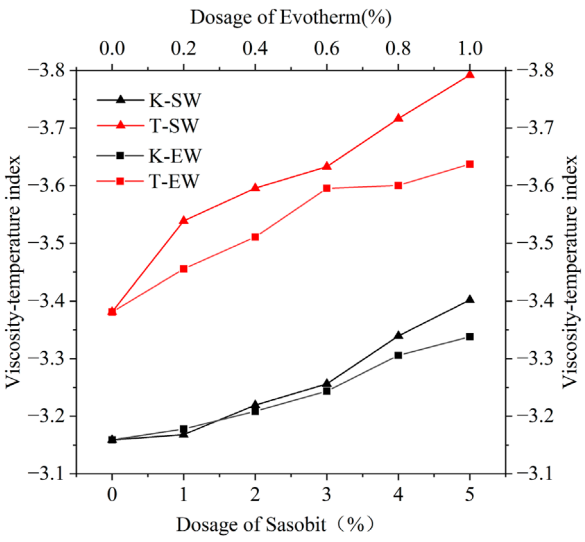

FIGURE 10
Viscosity-temperature index of base asphalt and WMA.

rose from 53.6 to 68.6, representing a percentage increase of 27.99%. Similarly, T-SW showed an increase from 57.5 to 72, with a percentage rise of 25.22%. This indicated that the inclusion of Sasobit improved the high-temperature performance of asphalt, enhanced its high-temperature stability. In comparison to Sasobit, Evotherm had a less pronounced effect on improving the high-temperature performance of asphalt, with softening point increases of 8.02% for K-EW and 4.39% for T-EW.

3.1.3 Ductility analysis

The experimental results for the ductility point of WMA were depicted in Figure 7B. The ductility values for T-EW and T-SW were both greater than 150 cm, therefore, they were not shown in the graph. From Figure 7B, it could be observed that the ductility of K-SW and K-EW showed no significant trend with an increase in the dosage of WMA. For T-SW and T-EW, their ductility values were both greater than 150, attributable to the better low-temperature deformation resistance of Tahe asphalt. Moreover, these values did not exhibit a clear pattern of change with an increase in the dosage of WMA. Therefore, ductility was not suitable for evaluating the low-temperature performance of WMA.

3.1.4 Viscosity temperature coefficient analysis

Figure 8 showed the viscosity curve of the base asphalt and WMA as a function of temperature.

It was observed in Figure 8 that the viscosity of WMA decreased with increasing temperature. This was because the molecular thermal motion inside asphalt accelerated with an increase in the external temperature, the intermolecular force decreased, and depolymerization occurred, which finally led to a decrease in the viscosity of asphalt.

Below 105°C, the viscosity of asphalt gradually increased with the addition of warm-mix additives at the same temperature for all four WMA types, except for T-EW. At temperatures above 105°C, at the same temperature, the viscosity of K90 was higher than that of K-SW, and the difference between their viscosities decreased with an increase in temperature. Simultaneously, the viscosity of K-SW gradually decreased with the addition of Sasobit dosage at the same temperature. The change in viscosity for K-EW and T-SW were minimally influenced by the dosage of warm-mix additives. Above 105°C, the viscosity trend of T-EW, in relation to the variation in warm-mix additive dosage, aligns with the trend seen in K-SW. Both K-SW and T-EW, classified as warm-mix asphalt types, experienced a decrease in viscosity. Two kinds of warm mixing asphalt, K-SW and T-EW, achieved the effect of reducing viscosity.

In this study, we used viscosity–temperature index VTS to analyze the temperature sensitivity of modified asphalt. The smaller the value, the higher the temperature sensitivity of the asphalt binders. Eq. 12 shows the VTS formula.

$$VTS = \frac{\lg[\lg(\eta_{T2}) - \lg(\eta_{T1})]}{\lg(T_2 + 273.13) - \lg(T_1 + 273.13)} \quad (12)$$

In Eq. 12, T_1 and T_2 are the test temperatures for the asphalt viscosity in °C; η_{T1} and η_{T2} are the viscosity values at temperatures T_1 and T_2, respectively, in Pa·s.

Figure 9 shows the VTS diagram of base asphalt and WMA, with the slope of the relation curve showing the VTS values of the WMA. Figure 9 summarizes the calculated results. The smaller the VTS of asphalt, the higher is the temperature sensitivity of the asphalt binder (Lu et al., 2022).

The data in Figure 10 suggest that the temperature sensitivity of Karamay asphalt was higher than that of Tahe asphalt. The temperature sensitivity of WMA modified with Evotherm is higher than that of WMA with Sasobit.

3.2 SARA analysis

According to the colloidal stability system, the lower the value of CII, the higher the asphaltene stability in asphalt binder. If CII ≥ 0.9, the asphaltene fraction was prone to instability within the crude oil. When at a level of 0.7 ≤ CII ≤ 0.9, asphaltene stability became uncertain, while if CII ≤ 0.7, the asphaltene fraction was stable (Siddiqui and Ali, 1999; Wang et al., 2019).

As shown in Figure 11, it was observed that the CII values of WMA remained within the original range, indicating that the addition of warm-mix additives had no discernible impact on the stability of the original asphaltene fraction.

Figure 11 illustrated the SARA fractions as well as the colloidal instability index for the base asphalt and WMA. The SARA fractions of K90 showed significant differences from common road asphalt, with very low Asphaltene (0.2%) and high Resins (45.46%). In comparison, binder T90 contained more Asphaltene (16.82%) and Aromatic (36.18%), but fewer Resins (19%) and Saturates (28%). This trend was attributed to the different oil source and refining process. The distinctive proportions of the SARA further highlighted the typicity of the two asphalts from Xinjiang. Furthermore, it was observed that the incorporation of the Warm mixing additive at a low dosage did not result in any significant changes in the ratio of the four asphalt components.

Figures 11A, C indicated that, as the concentration of Sasobit flux increased, the saturation hydrocarbon content gradually decreased. The wax structure of Sasobit was similar to the saturated

10.3389/fmats.2024.1363474

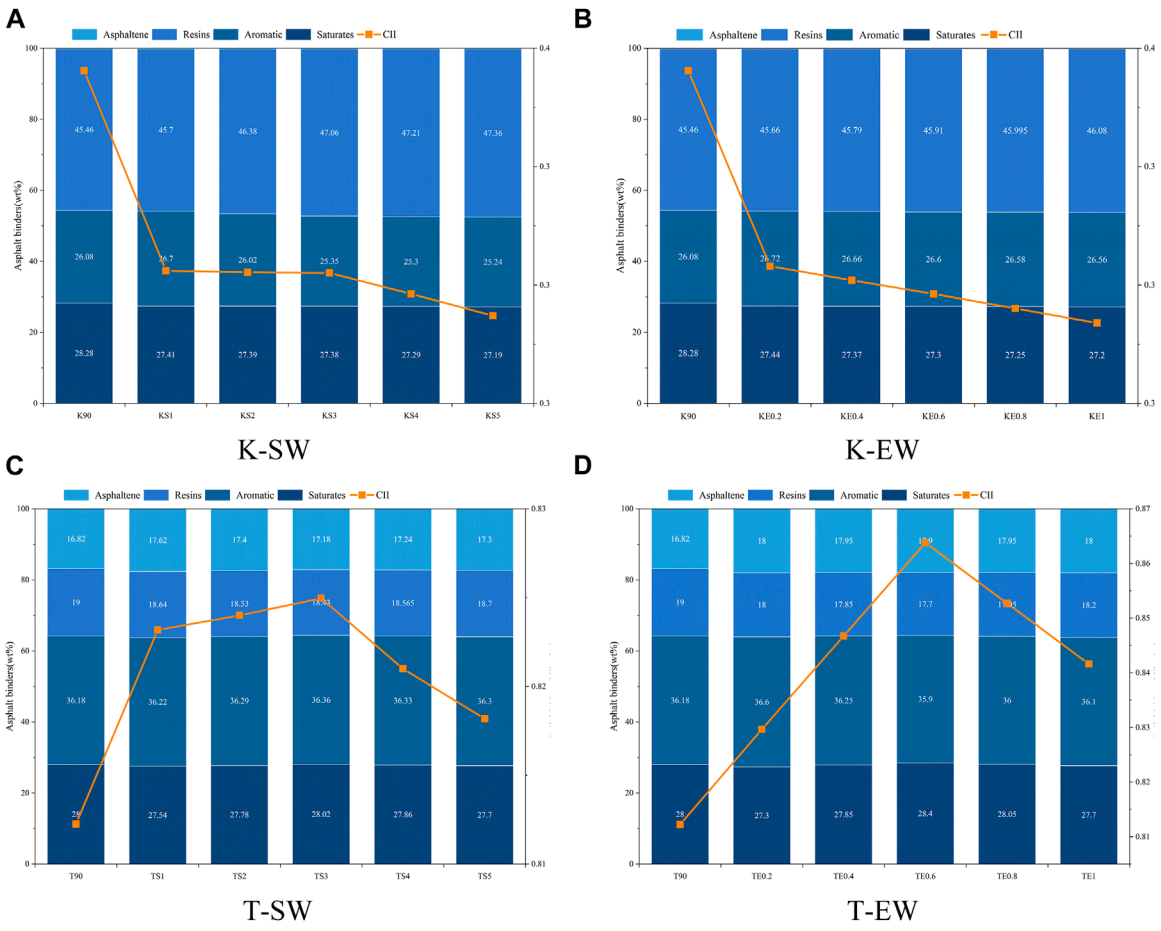

FIGURE 11
SARA fractions of base asphalt and WMA: **(A)** K-SW, **(B)** K-EW, **(C)** T-SW and **(D)** T-EW.

TABLE 5 Penetration correlation calculation table (Tahe asphalt).

ID	Penetration/0.1 mm			R2	PI	T_{800}/°C	$T_{1.2}$/°C
	15°C	20°C	25°C				
T90	38.3	92.2	137.1	0.999	0.507	50.50	−25.61
TS1	32.3	79.2	124.0	0.997	0.186	50.67	−21.92
TS2	29.9	74.0	116.0	0.999	0.118	51.30	−20.55
TS3	27.9	70.4	110.0	0.999	0.033	51.59	−19.36
TS4	25.5	66.0	104.0	0.999	−0.131	51.64	−17.56
TS5	24.1	60.2	100.0	0.999	−0.163	52.17	−16.70
TS0.2	38.0	91.6	136.1	0.997	0.507	50.60	−25.52
TS0.4	37.4	88.6	134.0	0.999	0.507	50.93	−25.40
TS0.6	36.3	84.1	130.1	0.999	0.526	51.42	−25.10
TS0.8	35.0	78.8	126.3	0.999	0.544	51.93	−24.59
TS 1	32.1	76.0	113.8	0.997	0.544	52.89	−23.85

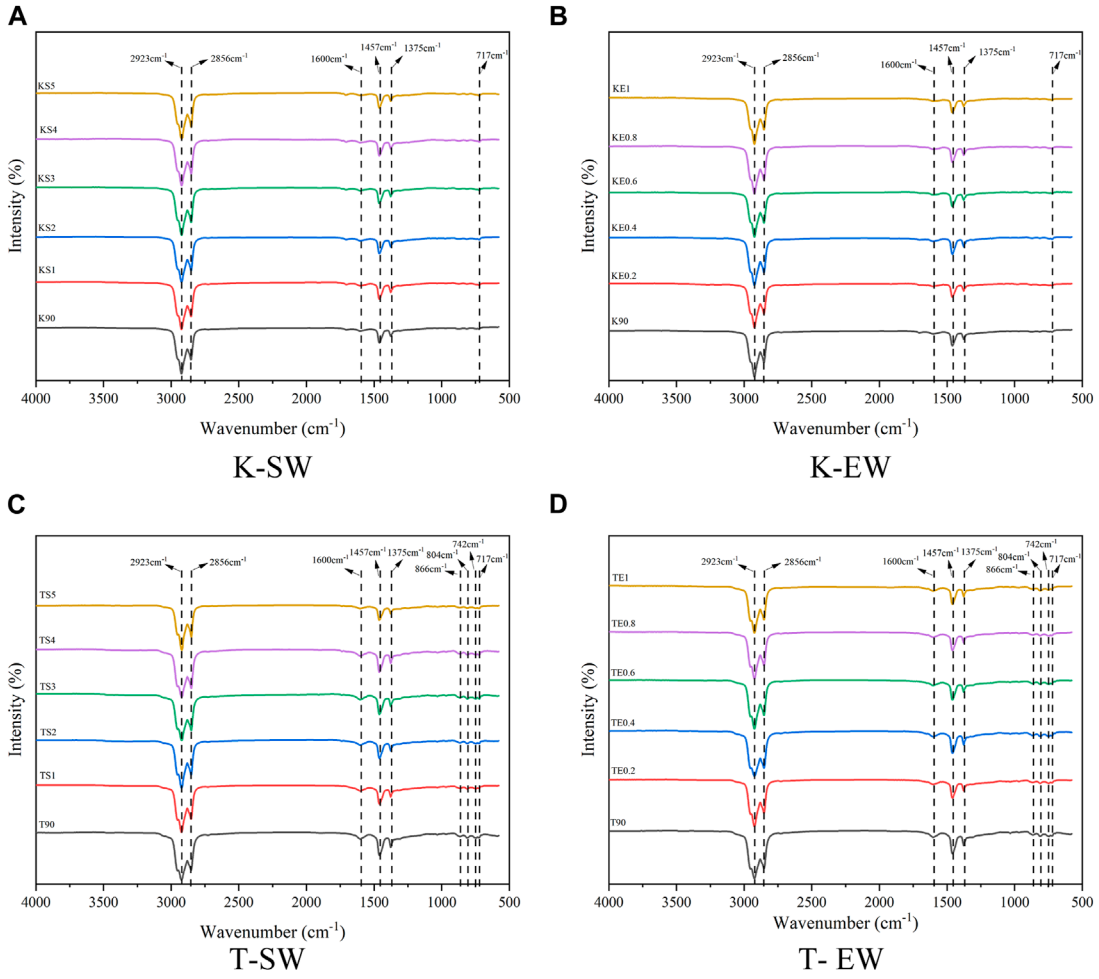

FIGURE 12
FTIR spectra of base asphalt and WMA: **(A)** K-SW, **(B)** K-EW, **(C)** T-SW and **(D)** T-EW.

TABLE 6 Solubility parameters of asphalt.

Asphalt type	K90	KS3	KE0.6	T90	TS3	TE0.6
CED(J/cm^3)	3.24	3.21	3.40	3.52	3.45	3.54
δ (J/cm^3)$^{1/2}$	18.00	17.92	18.44	18.77	18.57	18.81
$\Delta\delta$ (J/cm^3)$^{1/2}$	——	0.077	0.443	——	0.203	0.042

hydrocarbons in asphalt. When the temperature is below its melting point, Sasobit undergoes gradual crystallization and precipitation with the saturated component, effectively encapsulating saturated oil and wax components in the asphalt. This process enhances the high-temperature stability of the asphalt (Ji and Xu, 2010; Liu et al., 2019). During this process, the reagglomeration of resins or asphaltene was prevented (Butz et al., 2001; Abraham et al., 2002). Subsequently, the size of asphaltene aggregates was reduced, resulting in a decrease in the viscosity of the asphalt (Hurley and Prowell, 2005).

In K90 asphalt, where the asphaltene content is extremely low, the role of wax in binding asphaltene molecules is relatively small. Throughout the preparation of WMA, the base asphalt undergoes a certain degree of aging, leading to a decrease in the CII index of K-SW with an increase in the warm-mix additive (Figure 11A). In T90 asphalt, where the asphaltene content is relatively high, Sasobit effectively exerts its binding effect on asphaltene, resulting in the CII status as depicted in Figure 11C.

In the asphalt colloid system, the resins component exists in two states: it is both a component of the dispersed phase and a component of the dispersed medium (Li et al., 1997). Additionally, the polar components of the resin contain surface-active agents, exhibiting good compatibility with the cationic ammonium salt in Evotherm, resulting in a synergistic enhancement effect. This leads to an increase in asphaltene component, a decrease followed by an increase in resins (Lian et al., 1994). The structures of small molecules from Evotherm can enter the

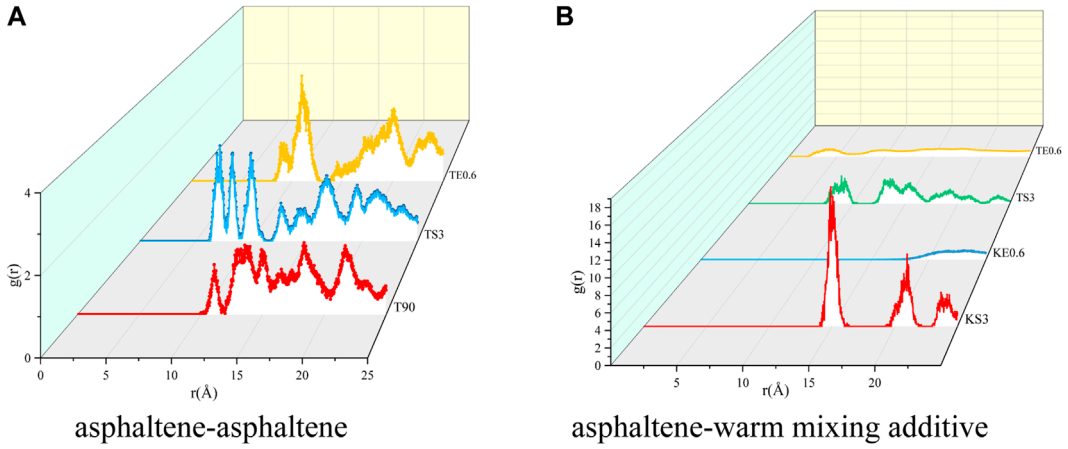

FIGURE 13
RDF of base asphalt and WMA: **(A)** asphaltene-asphaltene and **(B)** asphaltene-warm mixing additive.

aggregation gaps in asphaltene, preventing asphaltene binding and promoting the gelation of asphaltene colloids (Wang et al., 2023). In asphalts with a higher content of asphaltene and saturated fractions, the reactions with Evotherm can be fully realized. Therefore, in T-EW, the CII index exhibits a phenomenon of first increasing and then decreasing, with a turning point observed at an Evotherm content of 0.6% (Figure 11D). In K90 asphalt, due to the minimal presence of asphaltene in the asphalt, Evotherm primarily reacts with the saturated fractions. Consequently, the colloid content gradually increases in all four components, as illustrated in Figure 11B.

3.3 FTIR analysis

The FTIR spectra of base asphalt and WMA are shown in Figures 12A–D. The FTIR spectra of basic asphalt and WMA showed the same curve shape from 600cm^{-1}–4,000 cm^{-1}.The presence of saturated hydrocarbons (alkanes) is shown by the bands at 2923 cm^{-1} and 2856cm^{-1}, which are induced by asymmetrical and symmetrical stretching of -CH_2-, respectively. Furthermore, the bands around 1375 cm^{-1} show the symmetric distortion of C-H in CH_3, whereas the bands at roughly 717 cm^{-1} represent the stretching of C-H in CH_3 or CH_2. These bands could be seen in every FTIR spectrum, indicating that the asphalt binders and fractions had the same hydrocarbon components.

Furthermore, Aromatics, Resins, and Asphaltenes exhibited unique bands at roughly 810–860 cm^{-1} and 1600 cm^{-1} in Tahe asphalt and its warm mixed modified asphalt. These bands correspond to the = C-H and C=C stretching vibrations of benzene rings, respectively. This distinguishing trait strongly suggests that these three fractions have aromatic structures.

3.4 Molecular dynamics simulation results

In the MD simulation research process, the focus was on observing the motion and aggregation states of warm-mix additives in asphalt. Therefore, we have chosen five types of asphalt for the study, namely K90, KS3, KE0.6, T90, KS3, KE0.6.

3.4.1 Solubility parameter analysis

Table 6 displays the solubility parameters and the differences in solubility parameters between the base asphalt and WMA. According to the data, it is evident that in both Sasobit and Evotherm warm-mix additives, K90 exhibits better compatibility with Sasobit, while T90 shows better compatibility with Evotherm. This observation is consistent with the experimental conclusions drawn from the SARA.

3.4.2 RDF analysis

MD cohesion work is thought to be primarily governed by the aggregation behavior of asphalt molecules (Xu et al., 2018a). As a result, the RDF was used to learn more about how WMA additives affect asphalt molecule aggregation. Figure 12 depicts the RDF curves.

Figure 13A shows that the asphaltene-asphaltene RDF in the T90 base asphalt had a peak between 10Å and 12 Å, and the peak value was about 1, indicating that the particles in the local structure are uniformly distributed (Samieadel et al., 2018).The value of the first peak became larger and advance after adding Sasobit, the increase in the first peak value suggests that the packing density increased and the aggregation behavior of asphaltene was enhanced. The long-chain structure of Sasobit creates a higher probability of stacking of asphaltene molecules. The increase of asphaltene in SARA test was confirmed. Similarly, the early appearance of the TE0.6 wave crest in RDF also explains the increase of asphaltene in SARA test. Because K90 contains relatively little asphaltene, the results of asphaltene-asphaltene RDF are not presented here.

Figure 13B shows that the asphaltene-warm mixing additive RDF in the WMA. In K90 asphalt, the lower content of asphaltene molecules results in the delayed appearance of the KS3 peak between 14 Å and 16 Å, with a peak value of 18 indicating strong aggregation behavior between Sasobit molecules and asphaltene. The TE0.6 peak appears between 3 Å and 5 Å, and the subsequent curve remains in this range, indicating

a uniform distribution of Evotherm within this range and its role in dispersing asphaltene.

4 Conclusion

This paper clarifies the microscopic impact mechanisms of warm-mix additives by thoroughly characterizing the performance of WMA on numerous scales. The base asphalts selected are K90 and T90. Two typical warm-mix additives were investigated: wax-based WMA additive (Sasobit) and surfactant WMA additive (Evotherm). SARA component testing, infrared spectroscopy, and basic physical investigations were carried out. Warm mix additives' molecular impacts are revealed by the construction of molecular models and the execution of MD simulations for the representative WMA additives. Several inferences are made in light of the results that have been provided:

(1) Based on the T_{800} and $T_{1.2}$ indices, it was observed that K90 exhibited excellent low-temperature performance, while T90 demonstrated superior high-temperature characteristics. The incorporation of warm mix additives was found to effectively enhance both the high-temperature and low-temperature performance of asphalt. Notably, Evotherm proved to be more effective than Sasobit in improving the high-temperature performance of asphalt, whereas Sasobit surpassed Evotherm in its impact on low-temperature performance. The conclusions drawn from the VTS and PI metrics for warm mix asphalt were contradictory, prompting the exploration of alternative methods for evaluating the sensitivity of warm mix asphalt.

(2) Regarding the reduction in asphalt viscosity, it was observed that the variations in the dosage of warm mix additives had a negligible impact on the viscosity of warm mix asphalt. The viscosity-reducing effect of the Sasobit warm mix additive was found to be superior to that of Evotherm for K90, while for T90 asphalt, the situation was reversed.

(3) The analysis of warm mix additive mechanisms from the perspective of asphalt components, through both physical index tests and MD simulations, provided mutual validation. Sasobit, functioning as a wax-type warm mix additive, crystallized with the saturated components, forming a spatial network structure while facilitating the aggregation of asphaltene components. This conclusion was evident in the SARA analysis and the RDF in MD simulations. On the other hand, Evotherm warm mix additive, while dispersing asphaltene, also synergistically interacted with the polar components of resin. The reduction of asphalt content and resin in the SARA components validated this conclusion, with further clarification from the RDF in MD simulations.

(4) The Solubility parameter in MD simulations consistently aligns with the viscosity results of the asphalt. Concerning warm mix asphalt modification, it was observed that K90 asphalt exhibited better compatibility with Sasobit, while T90 asphalt was more suitable for modification with Evotherm.

Data availability statement

The original contributions presented in the study are included in the article/Supplementary material, further inquiries can be directed to the corresponding author.

Author contributions

BH: Writing–original draft, Methodology, Software, Investigation. XA: Conceptualization, Formal analysis, Supervision. JF: Writing–review and editing, Data curation, Formal analysis, Validation.

Funding

The author(s) declare financial support was received for the research, authorship, and/or publication of this article. The authors gratefully acknowledge the financial support provided by the Natural Science Foundation of Xinjiang Autonomous Region (Grant numbers: 2021D01C117 and 2022D01C396).

Conflict of interest

The authors declare that the research was conducted in the absence of any commercial or financial relationships that could be construed as a potential conflict of interest.

Publisher's note

All claims expressed in this article are solely those of the authors and do not necessarily represent those of their affiliated organizations, or those of the publisher, the editors and the reviewers. Any product that may be evaluated in this article, or claim that may be made by its manufacturer, is not guaranteed or endorsed by the publisher.

References

Abraham, J., Butz, T., Hildebrand, G., and Riebesehl, G. (2002). Asphalt flow improvers as' intelligent fillers' for hot asphalts-a new chapter in asphalt technology. *J. Appl. Asphalt Bind. Technol.* 2.

Banerjee, A., DE Fortier Smit, A., and Prozzi, J. A. (2012). The effect of long-term aging on the rheology of warm mix asphalt binders. *Fuel* 97, 603–611. doi:10.1016/j.fuel.2012.01.072

Brako, F., and Wexler, A. (1963). Determination of Functional Groups in Copolymers by Infrared Spectrometry. *Analytical Chemistry* 35, 1944–1947.

Butz, T., Rahimian, I., and Hildebrand, G. (2001). Modification of road bitumens with the Fischer-Tropsch paraffin Sasobit (R). *J. Appl. Asphalt Bind. Technol.* 1.

Cheng, L., Li, W., Chen, M., Qian, Z., Chen, X., and Zheng, Z. (2023). Bleeding mechanism and mitigation technique of basalt fiber-reinforced asphalt mixture. *Case Stud. Constr. Mater.* 19, e02442. doi:10.1016/j.cscm.2023.e02442

Cheng, L., Yu, J., Zhao, Q., Wu, J., and Zhang, L. (2020). Chemical, rheological and aging characteristic properties of Xinjiang rock asphalt-modified bitumen. *Constr. Build. Mater.* 240, 117908. doi:10.1016/j.conbuildmat.2019.117908

Chen, L., Liu, G., Pan, G., and Zhendong, Q. (2023a). Investigation on the pore water pressure in steel bridge deck pavement under the coupling effect of water and vehicle load. *Constr. Build. Mater.* 209, 134021. doi:10.1016/j.conbuildmat.2023.134021

Chen, L., Zhao, X., Qian, Z., and Li, X. (2023b). Mechanical behavior of asphalt pavement on steel-concrete composite beam bridge under temperature-load coupling. *Constr. Build. Mater.* 403, 133099. doi:10.1016/j.conbuildmat.2023.133099

Chen, Z., Pei, J., Li, R., and Xiao, F. (2018). Performance characteristics of asphalt materials based on molecular dynamics simulation – a review. *Constr. Build. Mater.* 189, 695–710. doi:10.1016/j.conbuildmat.2018.09.038

Eltwati, A., Al-Saffar, Z., Mohamed, A., Rosli Hainin, M., Elnihum, A., and Enieb, M. (2022). Synergistic effect of SBS copolymers and aromatic oil on the characteristics of asphalt binders and mixtures containing reclaimed asphalt pavement. *Constr. Build. Mater.* 327, 127026. doi:10.1016/j.conbuildmat.2022.127026

Gao, M., Chen, Y., Fan, C., and Li, M. (2022). Molecular dynamics study on the compatibility of asphalt and rubber powder with different component contents. *ACS Omega* 7, 36157–36164. doi:10.1021/acsomega.2c02813

Hansen, J. S., Lemarchand, C. A., Nielsen, E., Dyre, J. C., and SchrøDER, T. (2013). Four-component united-atom model of bitumen. *J. Chem. Phys.* 138, 094508. doi:10.1063/1.4792045

Hildebrand, J. H., and Scott, R. L. (1951). The solubility of nonelectrolytes (Hildebrand, joel H.). *J. Chem. Educ.* 29 (1), 51. doi:10.1021/ed029p51.1

Hossain, Z., Lewis, S., Zaman, M., Buddhala, A., and O'Rear, E. (2013). Evaluation for warm-mix additive-modified asphalt binders using spectroscopy techniques. *J. Mater. Civ. Eng.* 25, 149–159. doi:10.1061/(asce)mt.1943-5533.0000562

Hurley, G. C., and Prowell, B. D. (2005). Evaluation of Sasobit for use in warm mix asphalt. *NCAT Rep.* 5, 1–27.

Jiang, Q., Li, N., Yang, F., Ren, Y., Wu, S., Wang, F., et al. (2021). Rheology and volatile organic compounds characteristics of warm-mix flame retardant asphalt. *Constr. Build. Mater.* 298, 123691. doi:10.1016/j.conbuildmat.2021.123691

Ji, J., and Xu, S. 2010. Study on the impact of Sasobit on asphalt's properties and micro-structure. Pavements and Materials: Testing and Modeling in Multiple Length Scales.

Kim, H., Lee, S.-J., and Amirkhanian, S. N. (2011). Rheology of warm mix asphalt binders with aged binders. *Constr. Build. Mater.* 25, 183–189. doi:10.1016/j.conbuildmat.2010.06.040

Li, D. D., and Greenfield, M. L. (2014). Chemical compositions of improved model asphalt systems for molecular simulations. *Fuel* 115, 347–356. doi:10.1016/j.fuel.2013.07.012

Lian, H., Lin, J.-R., and Yen, T. F. (1994). Peptization studies of asphaltene and solubility parameter spectra. *Fuel* 73, 423–428. doi:10.1016/0016-2361(94)90097-3

Li, H., Liu, C., Kan, G., and Liang, W. (1997). Colloidal structure and formation of vacuum residual oil. *J. China Univ. Petroleum(Edition Nat. Sci.)* 21, 71–76.

Li, M., Min, Z., Wang, Q., Huang, W., and Shi, Z. (2022). Effect of epoxy resin content and conversion rate on the compatibility and component distribution of epoxy asphalt: a MD simulation study. *Constr. Build. Mater.* 319, 126050. doi:10.1016/j.conbuildmat.2021.126050

Liu, K., Zhu, J., Zhang, K., Wu, J., Yin, J., and Shi, X. (2019). Effects of mixing sequence on mechanical properties of graphene oxide and warm mix additive composite modified asphalt binder. *Constr. Build. Mater.* 217, 301–309. doi:10.1016/j.conbuildmat.2019.05.073

Lu, P., Ma, Y., Ye, K., and Huang, S. (2022). Analysis of high-temperature performance of polymer-modified asphalts through molecular dynamics simulations and experiments. *Constr. Build. Mater.* 350, 128903. doi:10.1016/j.conbuildmat.2022.128903

Masoumeh, M., Farideh, P., Daniel, O., Shahrzad, H., and Fini, E. H. (2016). Multiscale investigation of oxidative aging in biomodified asphalt binder. *J. Phys. Chem. C* 120 (31), 17224–17233. doi:10.1021/acs.jpcc.6b05004

Ning, A. M., Shen, B. X., Long, J., and Zhao, J. G. (2015). Comparison of the physical properties and chemical structures of the Tahe asphalt before and after oxidative aging. *Energy Sources, Part A Recovery, Util. Environ. Eff.* 37, 1495–1504. doi:10.1080/15567036.2011.621011

Oyan, M. N. S. (2022). *Feasibility assessment of warm mix asphalt in Arkansas*. Arkansas State, USA: Arkansas State University.

Rubio, M. C., MartíNEZ, G., Baena, L., and Moreno, F. (2012). Warm mix asphalt: an overview. *J. Clean. Prod.* 24, 76–84. doi:10.1016/j.jclepro.2011.11.053

Salehfard, R., Behbahani, H., Dalmazzo, D., and Santagata, E. (2021). Effect of colloidal instability on the rheological and fatigue properties of asphalt binders. *Constr. Build. Mater.* 281, 122563. doi:10.1016/j.conbuildmat.2021.122563

Samieadel, A., Oldham, D., and Fini, E. H. (2018). Investigating molecular conformation and packing of oxidized asphaltene molecules in presence of paraffin wax. *Fuel* 220, 503–512. doi:10.1016/j.fuel.2018.02.031

Sengoz, B., Topal, A., and Gorkem, C. (2013). Evaluation of natural zeolite as warm mix asphalt additive and its comparison with other warm mix additives. *Constr. Build. Mater.* 43, 242–252. doi:10.1016/j.conbuildmat.2013.02.026

Siddiqui, M. N., and Ali, M. F. (1999). Studies on the aging behavior of the Arabian asphalts. *Fuel* 78, 1005–1015. doi:10.1016/s0016-2361(99)00018-6

Topal, A., Sengoz, B., Kok, B. V., Yilmaz, M., Dokandari, P. A., Oner, J., et al. (2014). Evaluation of mixture characteristics of warm mix asphalt involving natural and synthetic zeolite additives. *Constr. Build. Mater.* 57, 38–44. doi:10.1016/j.conbuildmat.2014.01.093

Transport, E. D. O. C. J. O. H. A. (2020). Editorial department of China journal of highway and transport, 2020. Review on China's pavement engineering research-2020. *China J. Highw. Transp.* 33 (10), 1–66. (in Chinese). doi:10.19721/j.cnki.1001-7372.2020.10.001

Wang, C., Duan, K., Song, L., Ji, X., and Shu, C. (2022). Stability improvement technology of SBS/crumb rubber composite modified asphalt from Xinjiang China. *J. Clean. Prod.* 359, 132003. doi:10.1016/j.jclepro.2022.132003

Wang, J., Wang, T., Hou, X., and Xiao, F. (2019). Modelling of rheological and chemical properties of asphalt binder considering SARA fraction. *Fuel* 238, 320–330. doi:10.1016/j.fuel.2018.10.126

Wang, Y., Li, B., Li, D., Wei, D., Tu, C., Ren, X., et al. (2023). Effects of oxygen isolation and light–oxygen coupling ultraviolet aging on adhesion, micromorphology, and functional groups of warm-mix asphalt. *J. Mater. Civ. Eng.* 35, 04023309. doi:10.1061/jmcee7.mteng-15840

Wen, S. (2010). *Fourier transform infrared spectral analysis*. Peking, China: Chemical Industry Press.

Wu, M., Xu, G., Luan, Y., Zhu, Y., Ma, T., and Zhang, W. (2022). Molecular dynamics simulation on cohesion and adhesion properties of the emulsified cold recycled mixtures. *Constr. Build. Mater.* 333, 127403. doi:10.1016/j.conbuildmat.2022.127403

Xu, G., and Wang, H. (2016). Study of cohesion and adhesion properties of asphalt concrete with molecular dynamics simulation. *Comput. Mater. Sci.* 112, 161–169. doi:10.1016/j.commatsci.2015.10.024

Xu, G., Wang, H., and Sun, W. (2018a). Molecular dynamics study of rejuvenator effect on RAP binder: diffusion behavior and molecular structure. *Constr. Build. Mater.* 158, 1046–1054. doi:10.1016/j.conbuildmat.2017.09.192

Xu, T., Wang, Y., Xia, W., and Hu, Z. (2018b). Effects of flame retardants on thermal decomposition of SARA fractions separated from asphalt binder. *Constr. Build. Mater.* 173, 209–219. doi:10.1016/j.conbuildmat.2018.04.052

Yu, P., Ke-Hong, Y., XI-Xiong, L., and Xiang, L. (2018). The compatibility and stability mechanism of SBS modified Karamay asphalt. *Pet. Asph.* 32 (05), 25–32+37.

Yu, P., Liangquan, X., Wenshu, L., Nuerguli, (2019). Study of modification of Karamay asphalt by chemical method. *Petroleum Process. Petrochem.* 50 (03), 92–96.

Yusuff, A. O., Yahya, N., Zakariya, M. A., and Sikiru, S. (2021). Investigations of graphene impact on oil mobility and physicochemical interaction with sandstone surface. *J. Petroleum Sci. Eng.* 198, 108250. doi:10.1016/j.petrol.2020.108250

Yu, X., Wang, Y., and Luo, Y. (2013). Effects of types and content of warm-mix additives on CRMA. *J. Mater. Civ. Eng.* 25, 939–945. doi:10.1061/(asce)mt.1943-5533.0000765

Zhang, J., He, A., Wang, J., Zhang, Y., Yan, C., and Liu, Y. (2023). Study of bonding property of warm mix asphalt based on binder bond strength and molecular dynamics simulations. *J. Mater. Civ. Eng.* 35, 04023414. doi:10.1061/jmcee7.mteng-15678

Zhang, L., Cheng, L., Lu, Q., and Zhang, Z. (2023). Quantitative evaluation of asphalt blending characteristics in epoxy-modified hot recycled asphalt mixtures based on 3D confocal fluorescence technology. *J. Appl. Polym. Sci.*, e55073. doi:10.1002/app.55073

Zhang, L., and Greenfield, M. L. (2007). Relaxation time, diffusion, and viscosity analysis of model asphalt systems using molecular simulation. *J. Chem. Phys.* 127, 194502. doi:10.1063/1.2799189

Zhang, L., and Greenfield, M. L. (2008). Effects of polymer modification on properties and microstructure of model asphalt systems. *Energy & Fuels* 22, 3363–3375. doi:10.1021/ef700699p

Zhao, Y. (2012). Performance of warm-mix asphalt treated by quaternary ammonium salt surfactant. *J. Highw. Transp. Res. Dev.* 29 (8), 20–24.